

1 Convolutional neural networks can decode eye movement data: A black box approach to  
2 predicting task from eye movements

<sup>3</sup> Zachary J. Cole<sup>1</sup>, Karl M. Kuntzelman<sup>1</sup>, Michael D. Dodd<sup>1</sup>, & Matthew R. Johnson<sup>1</sup>

<sup>4</sup> <sup>1</sup> University of Nebraska-Lincoln

5 Author Note

The data used for the exploratory and confirmatory analyses in the present manuscript  
are derived from experiments funded by NIH/NEI Grant 1R01EY022974 to MDD. Work  
done to develop the analysis approach was supported by NSF/EPSCoR grant #1632849  
(MRJ and MDD). Additionally, this work was supported by the National Institute of General  
Medical Sciences of the National Institutes of Health [grant number P20 GM130461 awarded  
to MRJ and colleagues] and the Rural Drug Addiction Research Center at the University of  
Nebraska-Lincoln. The content is solely the responsibility of the authors and does not  
necessarily represent the official views of the National Institutes of Health or the University  
of Nebraska.

Correspondence concerning this article should be addressed to Zachary J. Cole, 238  
Burnett Hall, Lincoln, NE 68588-0308. E-mail: zachary@neurophysicole.com

17

## Abstract

18 Previous attempts to classify task from eye movement data have relied on model  
19 architectures designed to emulate theoretically defined cognitive processes, and/or data that  
20 has been processed into aggregate (e.g., fixations, saccades) or statistical (e.g., fixation  
21 density) features. *Black box* convolutional neural networks (CNNs) are capable of identifying  
22 relevant features in raw and minimally processed data and images, but difficulty interpreting  
23 the mechanisms underlying these model architectures has contributed to challenges in  
24 generalizing lab-trained CNNs to applied contexts. In the current study, a CNN classifier  
25 was used to classify task from two eye movement datasets (Exploratory and Confirmatory)  
26 in which participants searched, memorized, or rated indoor and outdoor scene images. The  
27 Exploratory dataset was used to tune the hyperparameters of the model, and the resulting  
28 model architecture was re-trained, validated, and tested on the Confirmatory dataset. The  
29 data were formatted into raw timeline data (i.e., x-coordinate, y-coordinate, pupil size) and  
30 minimally processed images. To further understand the relative informational value of the  
31 raw components of the eye movement data, the timeline and image datasets were broken  
32 down into subsets with one or more of the components of the data systematically removed.  
33 Average classification accuracies were compared between datasets and subsets. Classification  
34 of the timeline data consistently outperformed the image data. The Memorize condition was  
35 most often confused with the Search and Rate conditions. Pupil size was the least uniquely  
36 informative eye movement component when compared with the x- and y-coordinates. The  
37 general pattern of results for the Exploratory dataset was replicated in the Confirmatory  
38 dataset. Overall, the present study provides a practical and reliable black box solution to  
39 classifying task from eye movement data.

40

*Keywords:* deep learning, eye tracking, convolutional neural network, cognitive state,  
41 endogenous attention

42

## Introduction

43        The association between eye movements and mental activity is a fundamental topic of  
44      interest in attention research that has provided a foundation for developing a wide range of  
45      human assistive technologies. Early work by Yarbus (1967) showed that eye movement  
46      patterns appear to differ qualitatively depending on the task-at-hand (for a review of this  
47      work, see Tatler, Wade, Kwan, Findlay, & Velichkovsky, 2010). A replication of this work by  
48      DeAngelus and Pelz (2009) showed that the differences in eye movements between tasks can  
49      be quantified, and appear to be somewhat generalizable. Technological advances and  
50      improvements in computing power have allowed researchers to make inferences regarding the  
51      mental state underlying eye movement data, also known as the “inverse Yarbus process”  
52      (Haji-Abolhassani & Clark, 2014).

53        Current state-of-the-art machine learning and neural network algorithms are capable of  
54      identifying diagnostic patterns for the purpose of decoding a variety of data types, but the  
55      inner workings of the resulting model solutions are difficult or impossible to interpret.  
56      Algorithms that provide such solutions are referred to as *black box* models. Dissections of  
57      black box models have been largely uninformative (Zhou, Bau, Oliva, & Torralba, 2019),  
58      limiting the potential for researchers to apply the mechanisms underlying successful  
59      classification of the data. Still, black box models provide a powerful solution for  
60      technological applications such as human-computer interfaces (HCI; for a review, see  
61      Lukander, Toivanen, & Puolamäki, 2017). While the internal operations of the model  
62      solutions used for HCI applications do not necessarily need to be interpretable to serve their  
63      purpose, Lukander et al. (2017) pointed out that the inability to interpret the mechanisms  
64      underlying the function of black box solutions impedes the generalizability of these methods,  
65      and increases the difficulty of expanding these findings to real life applications. To ground  
66      these solutions, researchers guide decoding efforts by using eye movement data and/or  
67      models with built-in theoretical assumptions. For instance, eye movement data is processed

68 into meaningful aggregate properties such as fixations or saccades, or statistical features such  
69 as fixation density, and the models used to decode these data are structured based on the  
70 current understanding of relevant cognitive or neurobiological processes (e.g., MacInnes,  
71 Hunt, Clarke, & Dodd, 2018). Despite the proposed disadvantages of black box approaches  
72 to classifying eye movement data, there is no clear evidence to support the notion that the  
73 grounded solutions described above are actually more valid or definitive than a black box  
74 solution.

75 The scope of theoretically informed solutions to decoding eye movement data is limited  
76 to the extent of the current theoretical knowledge linking eye movements to cognitive and  
77 neurobiological processes. As our theoretical understanding of these processes develops, older  
78 theoretically informed models become outdated. Furthermore, these solutions are susceptible  
79 to any inaccurate preconceptions that are built into the theory. Consider the case of Greene,  
80 Liu, and Wolfe (2012), who were not able to classify task from commonly used aggregate eye  
81 movement features (i.e., number of fixations, mean fixation duration, mean saccade  
82 amplitude, percent of image covered by fixations) using correlations, a linear discriminant  
83 model, and a support vector machine (see Table 1). This led Greene and colleagues to  
84 question the robustness of Yarbus's (1967) findings, inspiring a slew of responses that  
85 successfully decoded the same dataset by aggregating the eye movements into different  
86 feature sets or implementing different model architectures (see Table 1; Haji-Abolhassani &  
87 Clark, 2014; Borji & Itti, 2014; Kanan, Ray, Bseiso, Hsiao, & Cottrell, 2014). The  
88 subsequent re-analyses of these data support Yarbus (1967) and the notion that mental state  
89 can be decoded from eye movement data using a variety of combinations of data features and  
90 model architectures. Collectively, these re-analyses did not point to an obvious global  
91 solution capable of clarifying future approaches to the inverse Yarbus problem beyond what  
92 could be inferred from black box model solutions, but did provide a wide-ranging survey of a  
93 variety of methodological features that can be applied to theoretical or black box approaches.

Eye movements can only delineate tasks to the extent that the cognitive processes underlying the tasks can be differentiated (Król & Król, 2018). Every task is associated with a unique set of cognitive processes (Coco & Keller, 2014; Król & Król, 2018), but in some cases, the cognitive processes for different tasks may produce indistinguishable eye movement patterns. To differentiate the cognitive processes underlying task-evoked eye movements, some studies have chosen to classify tasks that rely on stimuli that prompt easily distinguishable eye movements, such as reading text (e.g., Henderson, Shinkareva, Wang, Luke, & Olejarczyk, 2013). The eye movements elicited by salient stimulus features facilitate task classifications; however, because these eye movements are the consequence of a feature (or features) inherent to the stimulus rather than the task, it is unclear if these classifications are attributable to the stimulus or a complex mental state (e.g., Henderson et al., 2013; Boisvert & Bruce, 2016). Additionally, the distinct nature of exogenously elicited eye movements prompts decoding algorithms to prioritize these bottom-up patterns in the data over higher-level top-down effects (Borji & Itti, 2014). This means that these models are identifying the type of information that is being processed, but are not necessarily reflecting the mental state of the individual observing the stimulus. Eye movements that are the product of bottom-up processes have been reliably decoded, which is relevant for some HCI applications; however, such efforts do not fit the spirit of the inverse Yarbus problem, which is concerned with decoding high-level abstract mental operations that are not dependent on particular stimuli.

Currently, there is not a clearly established upper limit to how well cognitive task can be classified from eye movement data. Prior evidence has shown that the task-at-hand is capable of producing distinguishable eye movement features such as the total scan path length, total number of fixations, and the amount of time to the first saccade (Castelhano, Mack, & Henderson, 2009; DeAngelus & Pelz, 2009). Decoding accuracies within the context of determining task from eye movements typically range from chance performance to relatively robust classification (see Table 1). In one case, Coco and Keller (2014) categorized

the same eye movement features used by Greene et al. (2012) with respect to the relative contribution of latent visual or linguistic components of three tasks (visual search, name the picture, name objects in the picture) with 84% accuracy (chance = 33%). While this manipulation is reminiscent of other experiments relying on the bottom-up influence of words and pictures (e.g., Henderson et al., 2013; Boisvert & Bruce, 2016) the eye movements in the Coco and Keller (2014) tasks can be attributed to the occurrence of top-down attentional processes. A conceptually related follow-up to this study classified tasks along two spatial and semantic dimensions, resulting in 51% classification accuracy (chance = 25%; Król & Król, 2018). A closer look at these results showed that the categories within the semantic dimension were consistently misclassified, suggesting that this level of distinction may require a richer dataset, or a more powerful decoding algorithm. Altogether, there is no measurable index of relative top-down or bottom-up influence, but this body of literature suggests that the relative influence of top-down and bottom-up attentional processes may have a role in determining the decodability of the eye movement data.

As shown in Table 1, when eye movement data are prepared for classification, fixation and saccade statistics are typically aggregated along spatial or temporal dimensions, resulting in variables such as fixation density or saccade amplitude (Castelhano et al., 2009; MacInnes et al., 2018; Mills, Hollingworth, Van der Stigchel, Hoffman, & Dodd, 2011). The implementation of these statistical methods is meant to explicitly provide the decoding algorithm with characteristics of the eye movement data that are representative of theoretically relevant cognitive processes. For example, MacInnes et al. (2018) attempted to provide an algorithm with data designed to be representative of inputs to the frontal eye fields. In some instances, such as the case of Król and Król (2018), grounding the data using theoretically driven aggregation methods may require sacrificing granularity in the dataset. This means that aggregating the data has the potential to wash out certain fine-grained distinctions that could otherwise be detected. Data structures of any kind can only be decoded to the extent to which the data are capable of representing differences between

Table 1

*Previous Attempts to Classify Cognitive Task Using Eye Movement Data*

Study	Tasks	Features	Model Architecture	Accuracy (Chance)
Greene et al. (2012)	memorize, decade, people, wealth	number of fixations, mean fixation duration, mean saccade amplitude, percent of image covered by fixations, dwell times	linear discriminant, correlation, SVM	25.9% (25%)
Haji-Abolhassani & James (2014)	Greene et al. tasks	fixation clusters	Hidden Markov Models	59.64% (25%)
Kanan et al. (2014)	Greene et al. tasks	mean fixation durations, number of fixations	multi-fixation pattern analysis	37.9% (25%)
Borji & Itti (2014)	Greene et al. tasks	number of fixations, mean fixation duration, mean saccade amplitude, percent of image covered by fixations, first five fixations, fixation density	kNN, RUSBoost	34.34% (25%)
Borji & Itti (2014)	Yarbus tasks (i.e., view, wealth, age, prior activity, clothes, location, time away)	number of fixations, mean fixation duration, mean saccade amplitude, percent of image covered by fixations, first five fixations, fixation density	kNN, RUSBoost	24.21% (14.29%)
Coco & Keller (2014)	search, name picture, name object	Greene et al. features, latency of first fixation, first fixation duration, mean fixation duration, total gaze duration, initiation time, mean saliency at fixation, entropy of attentional landscape	MM, LASSO, SVM	84% (33%)
MacInnes et al. (2018)	view, memorize, search, rate	saccade latency, saccade duration, saccade amplitude, peak saccade velocity, absolute saccade angle, pupil size	augmented Naive Bayes Network	53.9% (25%)
Król & Król (2018)	people, indoors/outdoors, white/black, search	eccentricity, screen coverage	feed forward neural network	51.4% (25%)

<sup>148</sup> categories. Given that the cognitive processes underlying distinct tasks are often overlapping<sup>149</sup> (Coco & Keller, 2014), decreasing the granularity of the data may actually limit the potential

150 of the algorithm to make fine-grained distinctions between diagnostic components underlying  
151 the tasks to be decoded.

152 The current state of the literature does not provide any firm guidelines for determining  
153 what eye movement features are most meaningful, or what model architectures are best  
154 suited for determining mental state from eye movements. The examples provided in Table 1  
155 used a variety of eye movement features and model architectures, most of which were  
156 effective to some extent. A proper comparison of these outcomes is difficult because these  
157 datasets vary in levels of chance and data quality. Datasets with more tasks to be classified  
158 have lower levels of chance, lowering the threshold for successful classification. Additionally,  
159 datasets with a lower signal-to-noise ratio will have a lower achievable classification accuracy.  
160 For these reasons, outside of re-analyzing the same datasets, there is no consensus on how to  
161 establish direct comparisons of these model architectures. Given the inability to directly  
162 compare the relative effectiveness of the various theoretical approaches present in the  
163 literature, the current study addressed the inverse Yarbus problem by allowing a black box  
164 model to self-determine the most informative features from minimally processed eye  
165 movement data.

166 The current study explored pragmatic solutions to the problem of classifying task from  
167 eye movement data by submitting unprocessed x-coordinate, y-coordinate, and pupil size  
168 data to a convolutional neural network (CNN) model. Instead of transforming the data into  
169 theoretically defined units, we allowed the network to learn meaningful patterns in the data  
170 on its own. CNNs have a natural propensity to develop low-level feature detectors similar to  
171 the primary visual cortex (e.g., Seeliger et al., 2018); for this reason, they are commonly  
172 implemented for image classification. To test the possibility that the image data are better  
173 suited to the CNN classifier, the data were also transformed from raw timelines into simple  
174 image representations. To our knowledge, no study has attempted to address the inverse  
175 Yarbus problem using any combination of the following methods: (1) Non-aggregated data,

176 (2) image data format, and (3) a black-box CNN architecture. Given that CNN architectures  
177 are capable of learning features represented in raw data formats, and are well-suited to  
178 decoding multidimensional data that have a distinct spatial or temporal structure, we  
179 expected that a non-theoretically-constrained CNN architecture could be capable of decoding  
180 data at levels consistent with the current state of the art. Furthermore, despite evidence that  
181 black box approaches to the inverse Yarbus problem can impede generalizability (Lukander  
182 et al., 2017), we expected that when testing the approach on an entirely separate dataset,  
183 providing the model with minimally processed data and the flexibility to identify the unique  
184 features within each dataset would result in the replication of our initial findings.

185

## Method

186 **Participants**

187 Two separate datasets were used to develop and test the deep CNN architecture. The  
188 two datasets were collected from two separate experiments, which we refer to as Exploratory  
189 and Confirmatory. The participants for both datasets consisted of college students  
190 (Exploratory  $N = 124$ ; Confirmatory  $N = 77$ ) from the University of Nebraska-Lincoln who  
191 participated in exchange for class credit. Participants who took part in the Exploratory  
192 experiment did not participate in the Confirmatory experiment. All materials and  
193 procedures were approved by the University of Nebraska-Lincoln Institutional Review Board  
194 prior to data collection.

195 **Materials and Procedures**

196 Each participant viewed a series of indoor and outdoor scene images while carrying out  
197 a search, memorization, or rating task. For the memorization task, participants were  
198 instructed to memorize the image in anticipation of a forced choice recognition test. At the  
199 end of each Memorize trial, the participants were prompted to indicate which of two images  
200 was just presented. The two images were identical outside of a small change in the display

201 (e.g. object removed or added to the scene). For the rating task, participants were asked to  
202 think about how they would rate the image on a scale from 1 (very unpleasant) to 7 (very  
203 pleasant). The participants were prompted to provide a rating immediately after viewing the  
204 image. For the search task, participants were instructed to find a small “Z” or “N” embedded  
205 in the image. In reality, targets were not present in the images outside of a small subset of  
206 images ( $n = 5$ ) that were not analyzed but were included in the experiment design so  
207 participants believed a target was always present. Trials containing the target were excluded  
208 because search behavior was likely to stop if the target was found, adding considerable noise  
209 to the eye movement data. For consistency between trial types, participants were prompted  
210 to indicate if they found a “Z” or “N” at the end of each Search trial.

211 The same materials were used in both experiments with a minor variation in the  
212 procedures. In the Confirmatory experiment, participants were directed as to where search  
213 targets might appear in the image (e.g., on flat surfaces). No such instructions were provided  
214 in the Exploratory experiment.

215 In both experiments, participants completed one mixed block of 120 trials (task cued  
216 prior to each trial), or three uniform blocks of 40 trials (task cued prior to each block for a  
217 total of 120 trials). Block type was assigned in counterbalanced order. When the blocks were  
218 mixed, the trial types were randomly intermixed within the block. For uniform blocks, each  
219 block consisted entirely of one of the three conditions (Search, Memorize, Rate), with block  
220 types presented in random order. Each stimulus image was presented for 8 seconds. The  
221 pictures were presented in color, with a size of 1024 x 768 pixels, subtending a visual angle of  
222  $23.8^\circ \times 18.0^\circ$ .

223 Eye movements were recorded using an SR Research EyeLink 1000 eye tracker with a  
224 sampling rate of 1000Hz. Only the right eye was recorded. The system was calibrated using  
225 a nine-point accuracy and validity test. Errors greater than  $1^\circ$  or averaging greater than  $0.5^\circ$   
226 in total were re-calibrated.

227 **Datasets**

228 On some trials, a probe was presented on the screen six seconds after the onset of the  
229 trial which required participants to fixate the probe once detected. To avoid confounds  
230 resulting from the probe, only the first six seconds of the data for each trial was analyzed.  
231 Trials that contained fewer than 6000 samples within the first six seconds of the trial were  
232 excluded before analysis. For both datasets, the trials were pooled across participants. After  
233 excluding trials, the Exploratory dataset consisted of 12,177 of the 16,740 total trials, and  
234 the Confirmatory dataset consisted of 9,301 of the 10,395 total trials.

235 The raw x-coordinate, y-coordinate, and pupil size data collected at every sampling  
236 time point in the trial were used as inputs to the deep learning classifier. These data were  
237 also used to develop plot image datasets that were classified separately from the raw timeline  
238 datasets. For the plot image datasets, the timeline data for each trial were converted into  
239 scatterplot diagrams. The x- and y- coordinates and pupil size were used to plot each data  
240 point onto a scatterplot (e.g., see Figure 1). The coordinates were used to plot the location  
241 of the dot, pupil size was used to determine the relative size of the dot, and shading of the  
242 dot was used to indicate the time-course of the eye movements throughout the trial. The  
243 background of the plot images and first data point were white. Each subsequent data point  
244 was one shade darker than the previous data point until the final data point was reached.  
245 The final data point was black. For standardization, pupil size was divided by 10, and one  
246 unit was added. The plots were sized to match the dimensions of the data collection monitor  
247 (1024 x 768 pixels) and then shrunk to (240 x 180 pixels) in an effort to reduce the  
248 dimensionality of the data.

249 **Data Subsets.** The full timeline dataset was structured into three columns  
250 representing the x- and y- coordinates, and pupil size for each data point collected in the  
251 first six seconds of each trial. To systematically assess the predictive value of each XYP (i.e.,  
252 x-coordinates, y-coordinates, pupil size) component of the data, the timeline and image

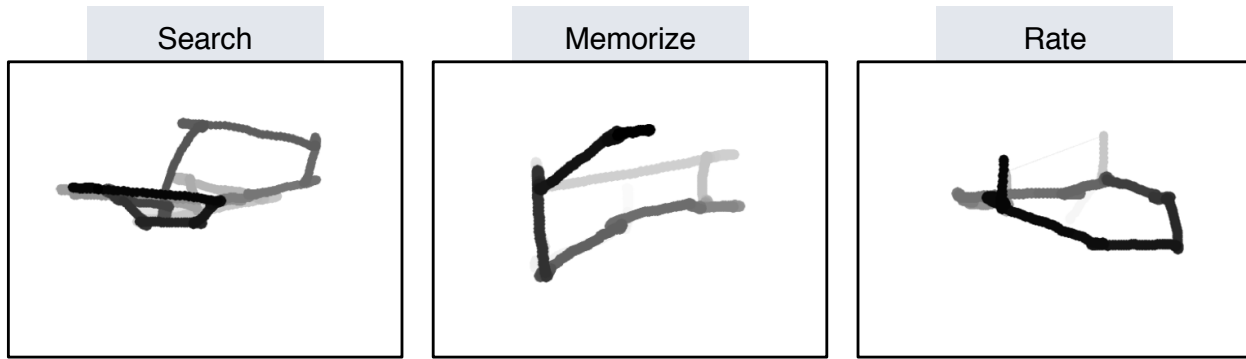


*Figure 1.* Each trial was represented as an image. Each sample collected within the trial was plotted as a dot in the image. Pupil size was represented by the size of the dot. The time course of the eye movements was represented by the gradual darkening of the dot over time.

253 datasets were batched into subsets that excluded one of the components (i.e., XYØ, XØP,  
 254 ØYP), or contained only one of the components (i.e., XØØ, ØYØ, ØØP). For the timeline  
 255 datasets, this means that the columns to be excluded in each data subset were replaced with  
 256 zeros. The data were replaced with zeros because removing the columns would change the  
 257 structure of the data. The same systematic batching process was carried out for the image  
 258 dataset. See Figure 2 for an example of each of these image data subsets.

259 **Classification**

260 Deep CNN model architectures were implemented to classify the trials into Search,  
 261 Memorize, or Rate categories. Because CNNs act as a digital filter sensitive to the number of  
 262 features in the data, the differences in the structure of the timeline and image data formats  
 263 necessitated separate CNN model architectures. The model architectures were developed  
 264 with the intent of establishing a generalizable approach to classifying cognitive processes  
 265 from eye movement data.

266 The development of these models was not guided by any formal theoretical  
 267 assumptions regarding the patterns or features likely to be extracted by the classifier. Like  
 268 many HCI models, the development of these models followed general intuitions concerned  
 269 with building a model architecture capable of transforming the data inputs into an  
 270 interpretable feature set that would not overfit the dataset. The models were developed

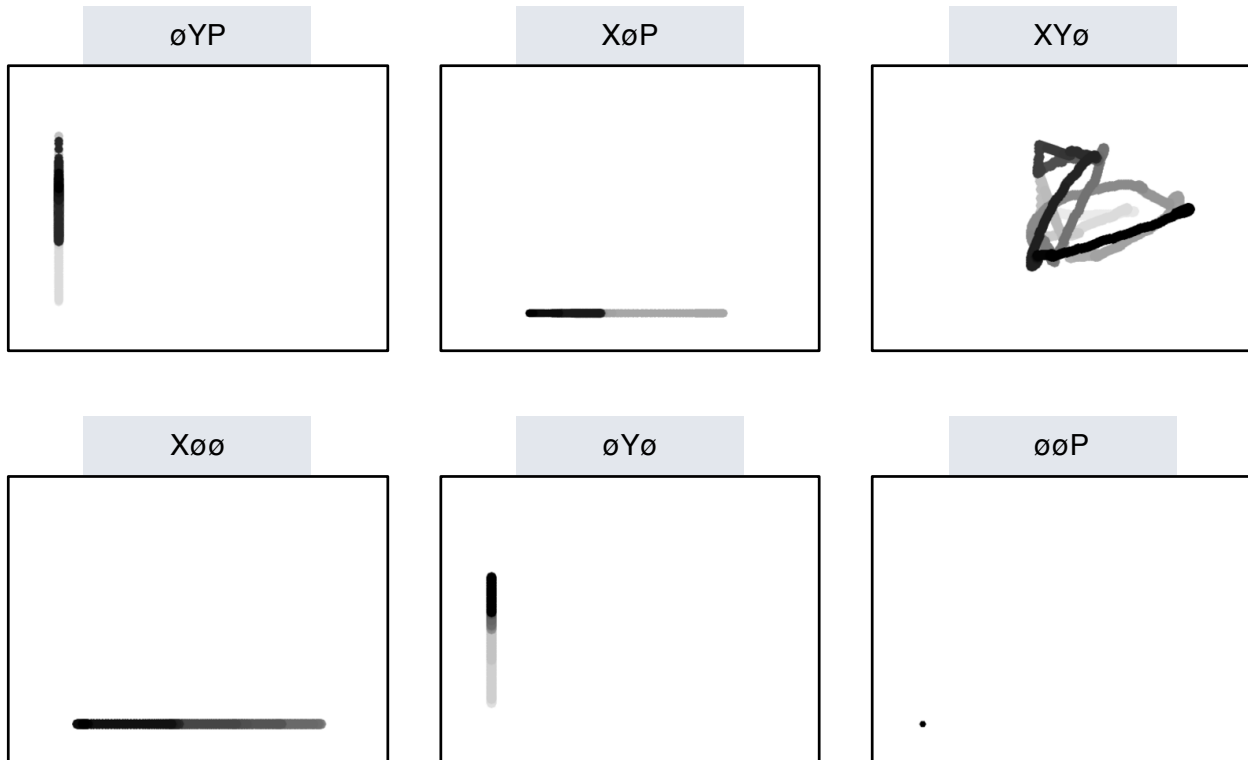


*Figure 2.* Plot images were used to represent data subsets that excluded one component of the eye movement data (i.e.,  $XY\emptyset$ ,  $X\emptyset\emptyset$ ,  $\emptyset YP$ ) or contained only one component (i.e.,  $X\emptyset\emptyset$ ,  $\emptyset Y\emptyset$ ,  $\emptyset\emptyset P$ ). As with the trials in the full  $XYP$  dataset, the time course of the eye movements was represented by the shading of the dot. The first sample of each trial was white, and the last sample was black.

271 using version 0.3b of the DeLINEATE toolbox, which operates over a Keras backend  
 272 (<http://delineate.it>; Kuntzman et al., under review). Each training/test iteration randomly  
 273 split the data so that 70% of the trials were allocated to training, 15% to validation, and  
 274 15% to testing. Training of the model was stopped when validation accuracy did not improve  
 275 over the span of 100 epochs. Once the early stopping threshold was reached, the resulting  
 276 model was tested on the held-out test data. This process was repeated 10 times for each  
 277 model, resulting in 10 classification accuracy scores for each model. The resulting accuracy  
 278 scores were used for the comparisons against chance and other datasets or data subsets.

279 The models were developed and tested on the Exploratory dataset. Model  
 280 hyperparameters were adjusted until the classification accuracies appeared to peak. The  
 281 model architecture with the highest classification accuracy on the Exploratory dataset was  
 282 trained, validated, and tested independently on the Confirmatory dataset. This means that

283 the model that was used to analyze the Confirmatory dataset was not trained on the  
284 Exploratory dataset. The model architectures used for the timeline and plot image datasets  
285 are shown in Figure 3.

## 286 Analysis

287 Results for the CNN architecture that resulted in the highest accuracy on the  
288 Exploratory dataset are reported below. For every dataset tested, a one-sample two-tailed  
289 *t*-test was used to compare the CNN accuracies against chance (33%). The Shapiro-Wilk test  
290 was used to assess the normality for each dataset. When normality was assumed, the mean  
291 accuracy for that dataset was compared against chance using Student's one-sample  
292 two-tailed *t*-test. When normality could not be assumed, the median accuracy for that  
293 dataset was compared against chance using Wilcoxon's Signed Rank test.

294 To determine the relative value of the three components of the eye movement data, the  
295 data subsets were compared within the timeline and plot image data types. If classification  
296 accuracies were lower when the data were batched into subsets, the component that was  
297 removed was assumed to have some unique contribution that the model was using to inform  
298 classification decisions. To determine the relative value of the contribution from each  
299 component, the accuracies from each subset with one component of the data removed were  
300 compared to the accuracies for the full dataset (XYP) using a one-way between-subjects  
301 Analysis of Variance (ANOVA). To further evaluate the decodability of each component  
302 independently, the accuracies from each subset containing only one component of the eye  
303 movement data were compared within a separate one-way between-subjects ANOVA. All  
304 post-hoc comparisons were corrected using Tukey's HSD.

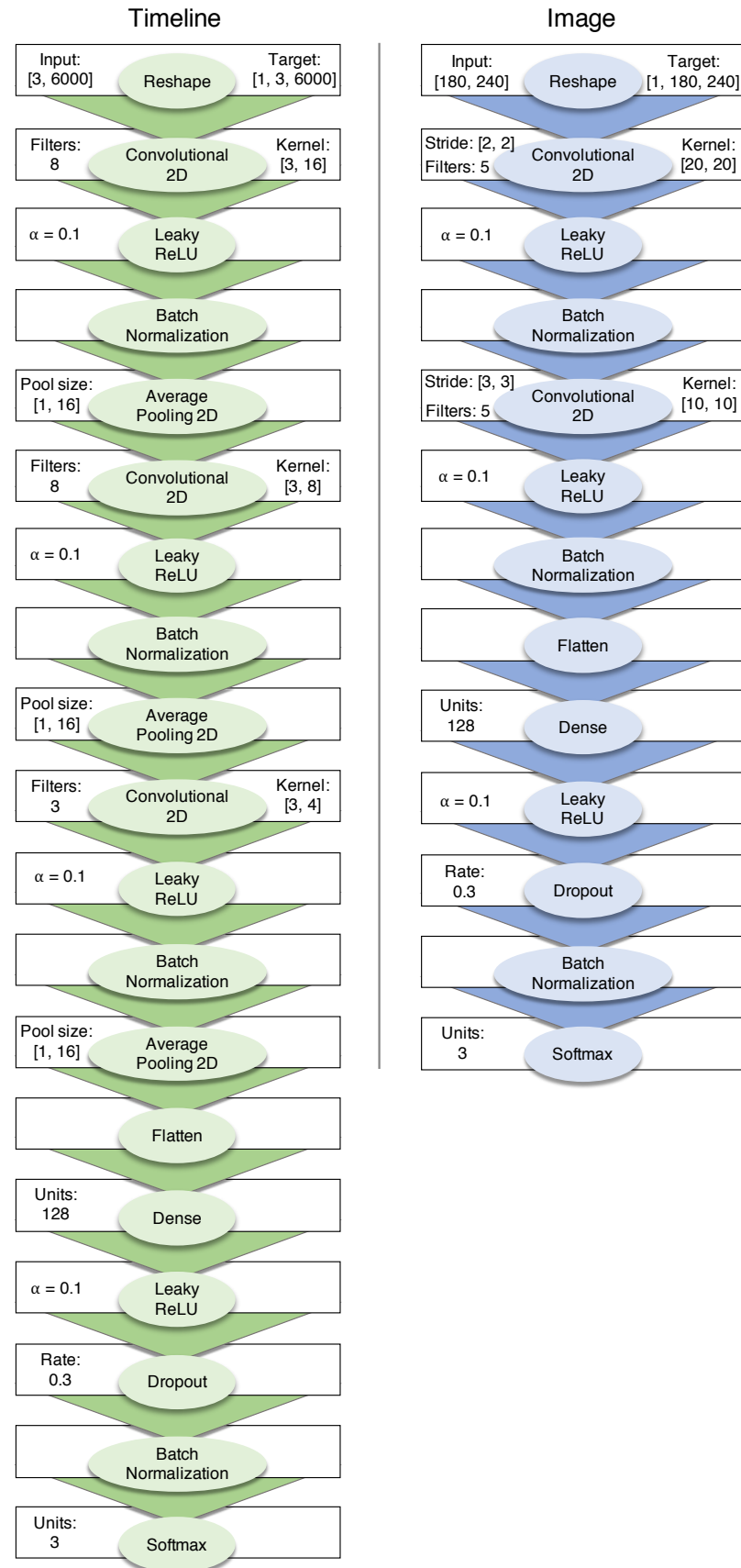


Figure 3. Two different model architectures were used to classify the timeline and image data. Both models were compiled using a categorical crossentropy loss function, and optimized with the Adam algorithm.

305

## Results

### 306 Timeline Data Classification

307       **Exploratory.** Classification accuracies for the XYP timeline dataset were well above  
 308 chance (chance = .33;  $M = .526$ ,  $SD = .018$ ;  $t_9 = 34.565$ ,  $p < .001$ ). Accuracies for  
 309 classifications of the batched data subsets were all better than chance (see Figure 4). As  
 310 shown in the confusion matrices displayed in Figure 5, the data subsets with lower overall  
 311 classification accuracies almost always classified the Memorize condition at or below chance  
 312 levels of accuracy. Misclassifications of the Memorize condition were split relatively evenly  
 313 between the Search and Rate conditions.

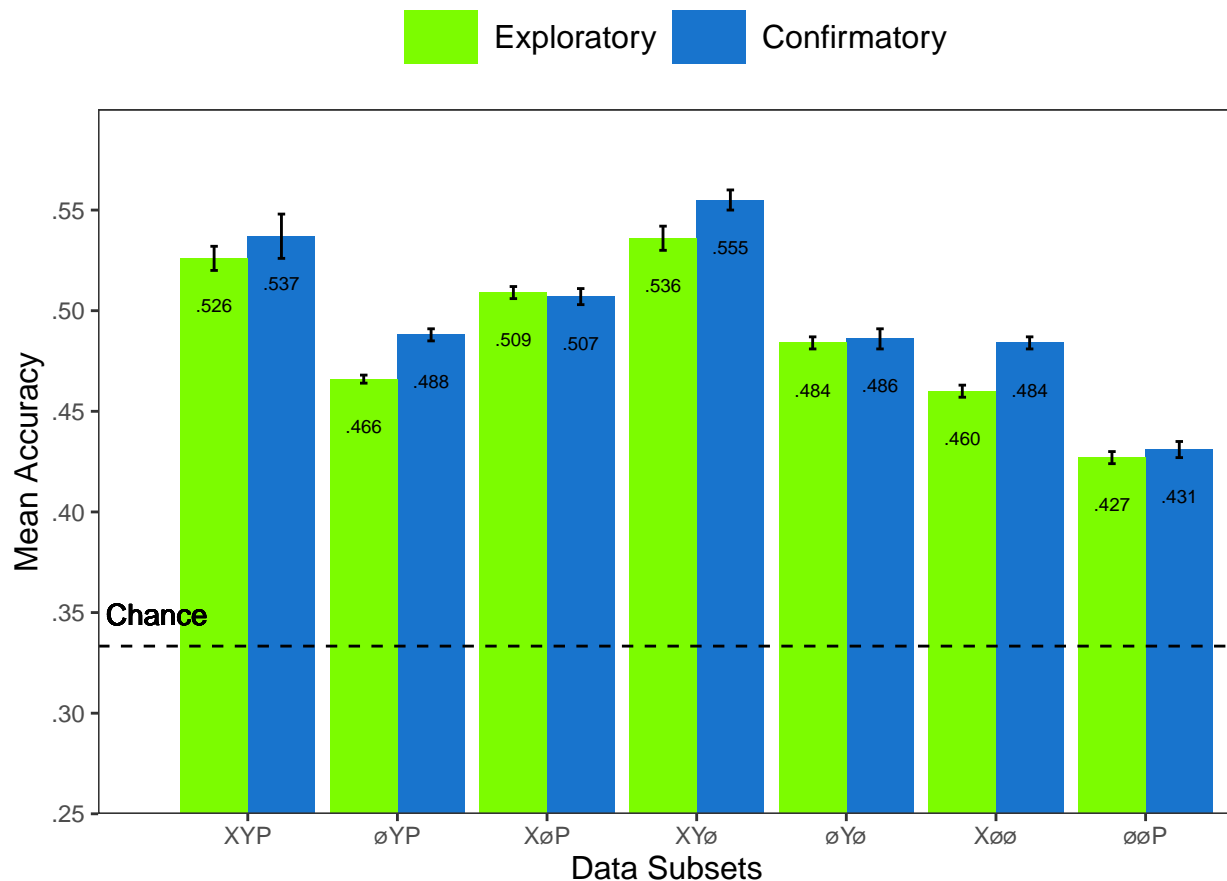


Figure 4. All of the data subsets were decoded at levels better than chance (.33). Each subset is labeled with the mean accuracy. The error bars represent standard errors.

314

There was a difference in classification accuracy for the XYP dataset and the subsets

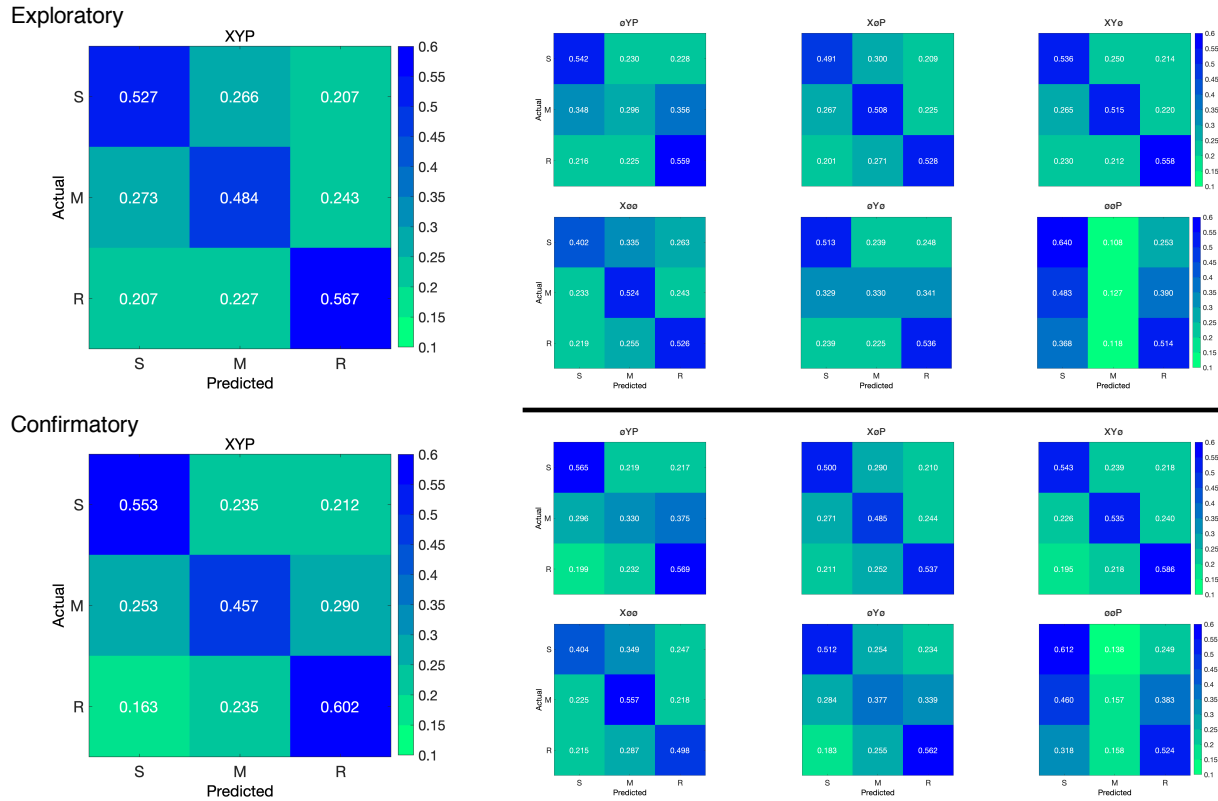


Figure 5. The confusion matrices represent the average classification accuracies for each condition of the timeline data (S = Search, M = Memorize, R = Rate). The vertical axis of the confusion matrices represents the actual condition for the trial. The horizontal axis of the confusion matrices represents the condition that was predicted by the model.

315 that had the pupil size, x-coordinate, and y-coordinate data systematically removed ( $F_{3,36} =$   
 316  $47.471, p < .001, \eta^2 = 0.798$ ). Post-hoc comparisons against the XYP dataset showed that  
 317 classification accuracies were not affected by the removal of pupil size or y-coordinate data  
 318 (see Table 2). The null effect present when pupil size was removed suggests that the pupil  
 319 size data were not contributing unique information that was not otherwise provided by the x-  
 320 and y-coordinates. A strict significance threshold of  $\alpha = .05$  implies the same conclusion for  
 321 the y-coordinate data, but the relatively low degrees of freedom ( $df = 18$ ) and the borderline  
 322 observed  $p$ -value ( $p = .056$ ) afford the possibility that there exists a small effect. However,  
 323 classification for the  $\emptyset$ YP subset was significantly lower than the XYP dataset, showing that  
 324 the x-coordinate data were uniquely informative to the classification.

325 There was also a difference in classification accuracies for the X $\emptyset\emptyset$ ,  $\emptyset$ Y $\emptyset$ , and  $\emptyset\emptyset$ P  
 326 subsets ( $F_{2,27} = 75.145, p < .001, \eta^2 = 0.848$ ). Post-hoc comparisons showed that

Table 2  
*Timeline Subset Comparisons*

Comparison	Exploratory		Confirmatory	
	t	p	t	p
XYP vs. $\emptyset$ YP	9.420	< .001	5.210	< .001
XYP vs. X $\emptyset$ P	2.645	.056	3.165	.016
XYP vs. XY $\emptyset$	1.635	.372	1.805	.288
X $\emptyset$ $\emptyset$ vs. $\emptyset$ Y $\emptyset$	5.187	< .001	0.495	.874
X $\emptyset$ $\emptyset$ vs. $\emptyset$ $\emptyset$ P	12.213	< .001	10.178	< .001
$\emptyset$ Y $\emptyset$ vs. $\emptyset$ $\emptyset$ P	7.026	< .001	9.683	< .001

classification accuracy for the  $\emptyset\emptyset$ P subset was lower than the X $\emptyset$  $\emptyset$  and  $\emptyset$ Y $\emptyset$  subsets.  
 Classification accuracy for the X $\emptyset$  $\emptyset$  subset was higher than the  $\emptyset$ Y $\emptyset$  subset. Altogether,  
 these findings suggest that pupil size data was the least uniquely informative to classification  
 decisions, while the x-coordinate data was the most uniquely informative.

**Confirmatory.** Classification accuracies for the Confirmatory XYP timeline dataset  
 were well above chance ( $M = .537$ ,  $SD = 0.036$ ,  $t_9 = 17.849$ ,  $p < .001$ ). Classification  
 accuracies for the data subsets were also better than chance (see Figure 4). Overall, there  
 was high similarity in the pattern of results for the Exploratory and Confirmatory datasets  
 (see Figure 4). Furthermore, the general trend showing that pupil size was the least  
 informative eye tracking data component was replicated in the Confirmatory dataset (see  
 Table 2). Also in concordance with the Exploratory timeline dataset, the confusion matrices  
 for these data revealed that the Memorize task was mis-classified more often than the Search  
 and Rate tasks (see Figure 5).

To test the generalizability of the model architecture, classification accuracies for the  
 XYP Exploratory and Confirmatory timeline datasets were compared. The Shapiro-Wilk  
 test for normality indicated that the Exploratory ( $W = 0.937$ ,  $p = .524$ ) and Confirmatory  
 ( $W = 0.884$ ,  $p = .145$ ) datasets were normally distributed, but Levene's test indicated that  
 the variances were not equal,  $F_{1,18} = 8.783$ ,  $p = .008$ . Welch's unequal variances  $t$ -test did  
 not show a difference between the two datasets,  $t_{13.045} = 0.907$ ,  $p = .381$ , Cohen's  $d = 0.406$ .

<sup>346</sup> These findings indicate that the deep learning model decoded the Exploratory and  
<sup>347</sup> Confirmatory timeline datasets equally well, but the Confirmatory dataset classifications  
<sup>348</sup> were less consistent across training/test iterations (as indicated by the increase in standard  
<sup>349</sup> deviation).

### <sup>350</sup> Plot Image Classification

<sup>351</sup> **Exploratory.** Classification accuracies for the XYP plot image data were better  
<sup>352</sup> than chance ( $M = .436$ ,  $SD = .020$ ,  $p < .001$ ), but were less accurate than the classifications  
<sup>353</sup> for the XYP Exploratory timeline data ( $t_{18} = 10.813$ ,  $p < .001$ ). Accuracies for the  
<sup>354</sup> classifications for all subsets of the plot image data except the  $\emptyset\emptyset P$  subset were better than  
<sup>355</sup> chance (see Figure 6). Following the pattern expressed by the timeline dataset, the confusion  
<sup>356</sup> matrices showed that the Memorize condition was misclassified more often than the other  
<sup>357</sup> conditions, and appeared to be equally mis-identified as a Search or Rate condition (see  
<sup>358</sup> Figure 7).

<sup>359</sup> There was a difference in classification accuracy between the XYP dataset and the data  
<sup>360</sup> subsets ( $F_{4,45} = 7.093$ ,  $p < .001$ ,  $\eta^2 = .387$ ). Post-hoc comparisons showed that compared to  
<sup>361</sup> the XYP dataset, there was no effect of removing pupil size or the x-coordinates, but  
<sup>362</sup> classification accuracy was worse when the y-coordinates were removed (see Table 3).

Table 3  
*Image Subset Comparisons*

Comparison	Exploratory		Confirmatory	
	<i>t</i>	<i>p</i>	<i>t</i>	<i>p</i>
XYP vs. $\emptyset YP$	1.792	.391	1.623	.491
XYP vs. $X\emptyset P$	2.939	.039	4.375	< .001
XYP vs. $XY\emptyset$	0.474	.989	1.557	.532
$X\emptyset\emptyset$ vs. $\emptyset Y\emptyset$	0.423	.906	2.807	.204
$X\emptyset\emptyset$ vs. $\emptyset\emptyset P$	13.569	< .001	5.070	< .001
$\emptyset Y\emptyset$ vs. $\emptyset\emptyset P$	13.235	< .001	7.877	< .001

<sup>363</sup> There was also a difference in classification accuracies between the  $X\emptyset\emptyset$ ,  $\emptyset Y\emptyset$ , and  
<sup>364</sup>  $\emptyset\emptyset P$  subsets (Levene's test:  $F_{2,27} = 3.815$ ,  $p = .035$ ; Welch correction for lack of

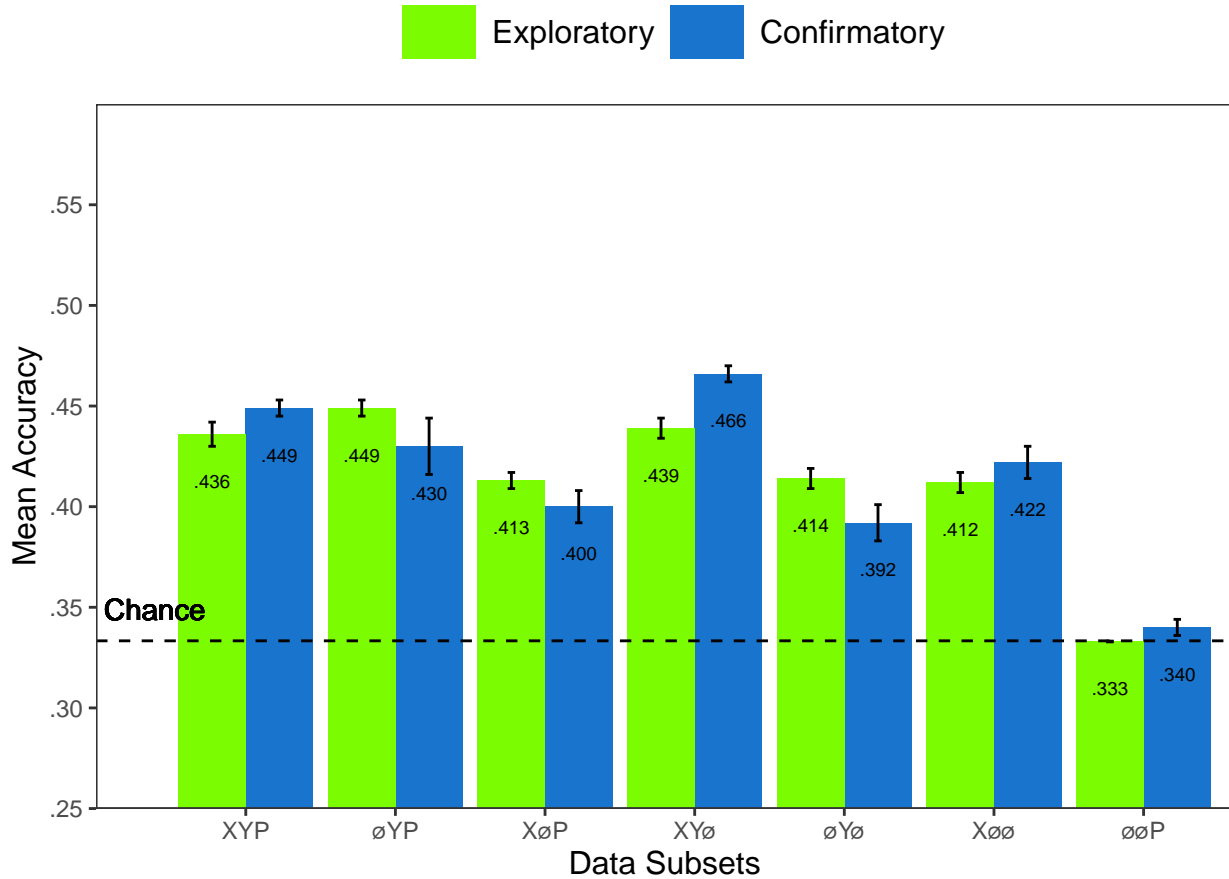


Figure 6. All of the data subsets except for the Exploratory ØØP dataset were decoded at levels better than chance (.33). Each subset is labeled with the mean accuracy. The error bars represent standard errors.

homogeneity of variances:  $F_{2,17.993} = 228.137, p < .001, \eta^2 = .899$ ). Post-hoc comparisons showed that there was no difference in classification accuracies for the XØØ and ØYØ subsets, but classification for the ØØP subset were less accurate than the XØØ and ØYØ subsets.

**Confirmatory.** Classification accuracies for the XYP confirmatory image dataset were well above chance ( $M = .449, SD = 0.012, t_9 = 31.061, p < .001$ ), but were less accurate than the classifications of the confirmatory timeline dataset ( $t_{18} = 11.167, p < .001$ ). Accuracies for classifications of the data subsets were also all better than chance (see Figure 6). The confusion matrices followed the pattern showing that the Memorize condition was mistaken most often, and was relatively equally mis-identified as a Search or Rate trial (see Figure 7). As with the timeline data, the general trend showing that pupil size data was

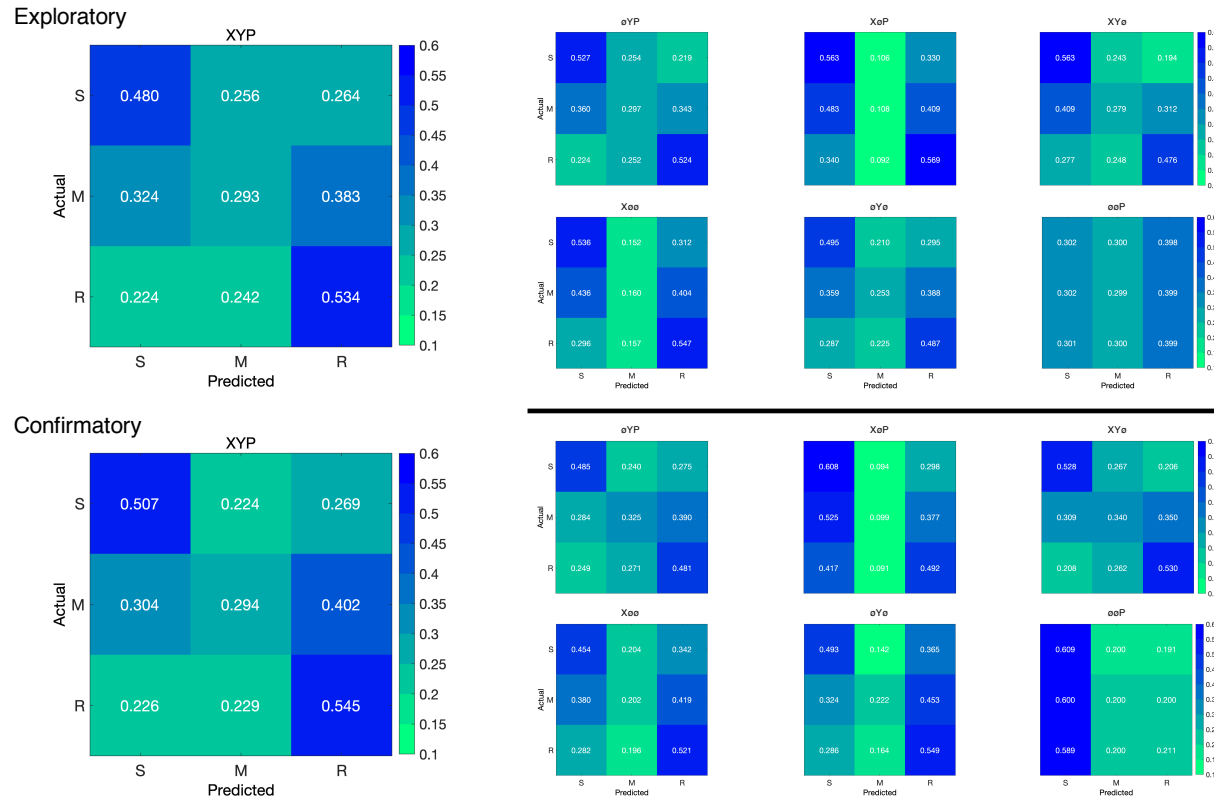


Figure 7. The confusion matrices represent the average classification accuracies for each condition of the image data (S = Search, M = Memorize, R = Rate). The vertical axis of the confusion matrices represents the actual condition for the trial. The horizontal axis of the confusion matrices represents the condition that was predicted by the model.

376 the least informative to the model was replicated in the Confirmatory dataset (see Table 3).

377 To test the generalizability of the model architecture, the classification accuracies for  
 378 the XYP Exploratory and Confirmatory plot image datasets were compared. The  
 379 independent samples *t*-test comparing the classification accuracies for the Exploratory and  
 380 Confirmatory plot image datasets did not show a significant difference,  $t_{18} = 1.777$ ,  $p = .092$ ,  
 381 Cohen's  $d = 0.795$ .

## 382 Discussion

383 The present study aimed to produce a practical and reliable example of a black box  
 384 solution to the inverse Yarbus problem. To implement this solution, we classified raw  
 385 timeline and minimally processed plot image data using a CNN model architecture. To our  
 386 knowledge, this study was the first to provide a solution to determining mental state from

387 eye movement data using each of the following: (1) Non-aggregated eye tracking data (i.e.,  
388 raw x-coordinates, y-coordinates, pupil size), (2) timeline and image data formats (see  
389 Figure 2), and (3) a black box CNN architecture. This study probed the relative predictive  
390 value of the x-coordinate, y-coordinate, and pupil size components of the eye movement data  
391 using a CNN. The CNN was able to decode the timeline and plot image data better than  
392 chance, although only the timeline datasets were decoded with accuracies comparable to  
393 other state-of-the-art approaches. Datasets with lower classification accuracies were not able  
394 to differentiate the cognitive processes underlying the Memorize task from the cognitive  
395 processes underlying the Search and Rate tasks. Decoding subsets of the data revealed that  
396 pupil size was the least uniquely informative component of the eye movement data. This  
397 pattern of findings was consistent between the Exploratory and Confirmatory datasets.

398 Although several aggregate eye movement features have been tested as task predictors,  
399 to our knowledge, no other study has assessed the predictive value of the data format (viz.,  
400 data in the format of a plot image). Our results suggest that although CNNs are robust  
401 image classifiers, eye movement data is decoded in the standard timeline format more  
402 effectively than in image format. This may be because the image data format contains less  
403 decodable information than the timeline format. Over the span of the trial (six seconds), the  
404 eye movements occasionally overlapped. When there was an overlap in the image data  
405 format, the more recent data points overwrote the older data points. This resulted in some  
406 information loss that did not occur when the data were represented in the raw timeline  
407 format. Despite this loss of information, the plot image format was still decoded with better  
408 than chance accuracy. To further examine the viability of classifying task from eye  
409 movement image datasets, future research might consider representing the data in different  
410 forms such as 3-dimensional data formats, or more complex color combinations capable of  
411 representing overlapping data points.

412 When considering the superior performance of the timeline data (vs., plot image data),

413 we must also consider the differences in the model architectures. Because the structures of  
414 the timeline and plot image data formats were different, the models decoding those data  
415 structures also needed to be different. Both model architectures were optimized individually  
416 on the Exploratory dataset before being tested on the Confirmatory dataset. For both  
417 timeline and plot image formats, there was good replicability between the Exploratory and  
418 Confirmatory datasets, demonstrating that these architectures performed similarly from  
419 experiment to experiment. An appropriately tuned CNN should be capable of learning any  
420 arbitrary function, but given that the upper bound for decodability of these datasets is  
421 unknown, there is the possibility that a model architecture exists that is capable of  
422 classifying the plot image data format more accurately than the model used to classify the  
423 timeline data. Despite this possibility, the convergence of these findings with other studies  
424 (see Table 1) suggests that the results of this study are approaching a ceiling for the  
425 potential to solve the inverse Yarbus problem with eye movement data. Although the true  
426 capacity to predict mental state from eye movement data is unknown, standardizing datasets  
427 in the future could provide a point for comparison that can more effectively indicate which  
428 methods are most effective at solving the inverse Yarbus problem.

429 In the current study, the Memorize condition was classified less accurately than the  
430 Search and Rate conditions, especially for the datasets with lower overall accuracy. This  
431 suggests that the eye movements associated with the Memorize task were potentially lacking  
432 unique or informative features to decode. This means that eye movements associated with  
433 the Memorize condition were interpreted as noise, or were sharing features of underlying  
434 cognitive processes that were represented in the eye movements associated with the Search  
435 and Rate tasks. Previous research (e.g., Król & Król, 2018) has attributed the inability to  
436 differentiate one condition from the others to the overlapping of sub-features in the eye  
437 movements between two tasks that are too subtle to be represented in the eye movement  
438 data.

439 To more clearly understand how the different tasks influenced the decodability of the  
440 eye movement data, additional analyses were conducted on the Exploratory and  
441 Confirmatory timeline datasets (see Appendix). For the main supplementary analysis, the  
442 data subsets were re-submitted to the CNN and re-classified as 2-category task sets. In  
443 addition to the main supplementary analysis, the results from the primary analysis were  
444 re-calculated from 3-category task sets to 2-category task sets. In the primary analyses, the  
445 Memorize condition was predicted with the lowest accuracy, but mis-classifications of the  
446 Search and Rate trials were most often categorized as Memorize. As a whole, this pattern of  
447 results and the main supplementary analysis indicated a general bias for uncertain trials to  
448 be categorized as Memorize. As expected, the main supplementary analysis also showed that  
449 the 2-category task set that included only Search and Rate had higher accuracies than both  
450 of the 2-category task sets that included the Memorize condition. The re-calculation analysis  
451 generally replicated the pattern of results seen in the main supplementary analysis but with  
452 larger variance, suggesting that including lower-accuracy trial types during model training  
453 can decrease the consistency of classifier performance. Overall, the findings from this  
454 supplemental analysis show that conclusions drawn from comparisons between approaches  
455 that do not use the same task sets, or the same number of tasks, could be potentially  
456 uninterpretable because the features underlying the task categories are interpreted differently  
457 by the neural network algorithm.

458 When determining the relative contributions of the the eye movement features used in  
459 this study (x-coordinates, y-coordinates, pupil size), the pupil size data was consistently the  
460 least uniquely informative. When pupil size was removed from the Exploratory and  
461 Confirmatory timeline and plot image datasets, classification accuracy remained stable (vs.,  
462 XYP dataset). Furthermore, classification accuracy of the  $\emptyset\emptyset\emptyset$  subset was the lowest of all  
463 of the data subsets, and in one instance, was no better than chance. Although these findings  
464 indicate that, in this case, pupil size was a relatively uninformative component of the eye  
465 movement data, previous research has associated changes in pupil size as indicators of

466 working memory load (Kahneman & Beatty, 1966; Karatekin, Couperus, & Marcus, 2004),  
467 arousal (Wang et al., 2018), and cognitive effort (Porter, Troscianko, & Gilchrist, 2007). The  
468 results of the current study indicate that the changes in pupil size associated with these  
469 underlying processes were not useful in delineating the tasks being classified (i.e., Search,  
470 Memorize, Rate), potentially because these tasks did not evoke a reliable pattern of changes  
471 in pupil size. Additionally, properties of the stimuli known to influence pupil size, such as  
472 luminance and contrast, were not controlled in these datasets. Given that stimuli were  
473 randomly assigned, there is the possibility that uncontrolled stimulus properties known to  
474 affect pupil size impeded the CNN's capacity to detect patterns in the pupil size data.

475 The findings from the current study support the notion that black box CNNs are a  
476 viable approach to determining task from eye movement data. In a recent review, Lukander  
477 et al. (2017) expressed concern regarding the lack of generalizability of black box approaches  
478 when decoding eye movement data. Overall, the current study showed a consistent pattern  
479 of results for the XYP timeline and image datasets, but some minor inconsistencies in the  
480 pattern of results for the x- and y- coordinate subset comparisons. These inconsistencies may  
481 be a product of overlap in the cognitive processes underlying the three tasks. When the data  
482 are batched into subsets, at least one dimension (i.e., x-coordinates, y-coordinates, or pupil  
483 size) is removed, leading to a potential loss of information. When the data provide fewer  
484 meaningful distinctions, finer-grained inferences are necessary for the tasks to be  
485 distinguishable. As shown by Coco and Keller (2014), eye movement data can be more  
486 effectively decoded when the cognitive processes underlying the tasks are explicitly  
487 differentiable. While the cognitive processes distinguishing memorizing, searching, or rating  
488 an image are intuitively different, the eye movements elicited from these cognitive processes  
489 are not easily differentiated. To correct for potential mismatches between the distinctive  
490 task-diagnostic features in the data and the level of distinctiveness required to classify the  
491 tasks, future research could more definitively conceptualize the cognitive processes  
492 underlying the task-at-hand.

493 Classifying mental state from eye movement data is often carried out in an effort to

494 advance technology to improve educational outcomes, strengthen the independence of

495 physically and mentally handicapped individuals, or improve HCI's (Koochaki &

496 Najafizadeh, 2018). Given the previous questions raised regarding the reliability and

497 generalizability of black-box CNN classification, the current study first tested models on an

498 exploratory dataset, then confirmed the outcome using a second independent dataset.

499 Overall, the findings of this study indicate that this black-box approach is capable of

500 producing a stable and generalizable outcome. Additionally, the supplementary analyses

501 showed that different task sets, or a different number of tasks, could lead the algorithm to

502 interpret features differently, which should be taken into account when comparing task

503 classification approaches. Future studies that incorporate features from the stimulus might

504 have the potential to surpass current state-of-the-art classification. According to Bulling,

505 Weichel, and Gellersen (2013), incorporating stimulus feature information into the dataset

506 may improve accuracy relative to decoding gaze location data and pupil size. Alternatively,

507 Borji and Itti (2014) suggested that accounting for salient features in the the stimulus might

508 leave little to no room for theoretically defined classifiers to consider mental state. Future

509 research should examine the potential for the inclusion of stimulus feature information in

510 addition to the eye movement data to boost black-box CNN classification accuracy of image

511 data beyond that of timeline data.

512

## References

- 513 Boisvert, J. F. G., & Bruce, N. D. B. (2016). Predicting task from eye movements: On the  
514 importance of spatial distribution, dynamics, and image features. *Neurocomputing*,  
515 207, 653–668. <https://doi.org/10.1016/j.neucom.2016.05.047>
- 516 Borji, A., & Itti, L. (2014). Defending Yarbus: Eye movements reveal observers' task.  
517 *Journal of Vision*, 14(3), 1–21. <https://doi.org/10.1167/14.3.29>
- 518 Bulling, A., Weichel, C., & Gellersen, H. (2013). EyeContext: Recognition of high-level  
519 contextual cues from human visual behaviour. In *Proceedings of the SIGCHI  
520 Conference on Human Factors in Computing Systems - CHI '13* (p. 305). Paris,  
521 France: ACM Press. <https://doi.org/10.1145/2470654.2470697>
- 522 Castelhano, M. S., Mack, M. L., & Henderson, J. M. (2009). Viewing task influences eye  
523 movement control during active scene perception. *Journal of Vision*, 9(3), 1–15.  
524 <https://doi.org/10.1167/9.3.6>
- 525 Coco, M. I., & Keller, F. (2014). Classification of visual and linguistic tasks using  
526 eye-movement features. *Journal of Vision*, 14(3), 1–18.  
527 <https://doi.org/10.1167/14.3.11>
- 528 DeAngelus, M., & Pelz, J. B. (2009). Top-down control of eye movements: Yarbus revisited.  
529 *Visual Cognition*, 17(6-7), 790–811. <https://doi.org/10.1080/13506280902793843>
- 530 Greene, M. R., Liu, T., & Wolfe, J. M. (2012). Reconsidering Yarbus: A failure to predict  
531 observers' task from eye movement patterns. *Vision Research*, 62, 1–8.  
532 <https://doi.org/10.1016/j.visres.2012.03.019>
- 533 Haji-Abolhassani, A., & Clark, J. J. (2014). An inverse Yarbus process: Predicting observers'  
534 task from eye movement patterns. *Vision Research*, 103, 127–142.

- 535 <https://doi.org/10.1016/j.visres.2014.08.014>
- 536 Henderson, J. M., Shinkareva, S. V., Wang, J., Luke, S. G., & Olejarczyk, J. (2013).  
537 Predicting Cognitive State from Eye Movements. *PLoS ONE*, 8(5), e64937.  
538 <https://doi.org/10.1371/journal.pone.0064937>
- 539 Kahneman, D., & Beatty, J. (1966). Pupil Diameter and Load on Memory. *Science*,  
540 154(3756), 1583–1585. Retrieved from <http://www.jstor.org/stable/1720478>
- 541 Kanan, C., Ray, N. A., Bseiso, D. N. F., Hsiao, J. H., & Cottrell, G. W. (2014). Predicting  
542 an observer's task using multi-fixation pattern analysis. In *Proceedings of the*  
543 *Symposium on Eye Tracking Research and Applications - ETRA '14* (pp. 287–290).  
544 Safety Harbor, Florida: ACM Press. <https://doi.org/10.1145/2578153.2578208>
- 545 Karatekin, C., Couperus, J. W., & Marcus, D. J. (2004). Attention allocation in the  
546 dual-task paradigm as measured through behavioral and psychophysiological  
547 responses. *Psychophysiology*, 41(2), 175–185.  
548 <https://doi.org/10.1111/j.1469-8986.2004.00147.x>
- 549 Koochaki, F., & Najafizadeh, L. (2018). Predicting Intention Through Eye Gaze Patterns.  
550 In *2018 IEEE Biomedical Circuits and Systems Conference (BioCAS)* (pp. 1–4).  
551 <https://doi.org/10.1109/BIOCAS.2018.8584665>
- 552 Król, M. E., & Król, M. (2018). The right look for the job: Decoding cognitive processes  
553 involved in the task from spatial eye-movement patterns. *Psychological Research*, 84,  
554 245–258. <https://doi.org/10.1007/s00426-018-0996-5>
- 555 Lukander, K., Toivanen, M., & Puolamäki, K. (2017). Inferring Intent and Action from Gaze  
556 in Naturalistic Behavior: A Review. *International Journal of Mobile Human*  
557 *Computer Interaction*, 9(4), 41–57. <https://doi.org/10.4018/IJMHCI.2017100104>

- 558 MacInnes, W., Joseph, Hunt, A. R., Clarke, A. D. F., & Dodd, M. D. (2018). A Generative  
559 Model of Cognitive State from Task and Eye Movements. *Cognitive Computation*,  
560 10(5), 703–717. <https://doi.org/10.1007/s12559-018-9558-9>
- 561 Mills, M., Hollingworth, A., Van der Stigchel, S., Hoffman, L., & Dodd, M. D. (2011).  
562 Examining the influence of task set on eye movements and fixations. *Journal of*  
563 *Vision*, 11(8), 1–15. <https://doi.org/10.1167/11.8.17>
- 564 Porter, G., Troscianko, T., & Gilchrist, I. D. (2007). Effort during visual search and  
565 counting: Insights from pupillometry. *Quarterly Journal of Experimental Psychology*  
566 (2006), 60(2), 211–229. <https://doi.org/10.1080/17470210600673818>
- 567 Seeliger, K., Fritzsche, M., Güçlü, U., Schoenmakers, S., Schoffelen, J.-M., Bosch, S. E., &  
568 van Gerven, M. A. J. (2018). Convolutional neural network-based encoding and  
569 decoding of visual object recognition in space and time. *NeuroImage*, 180, 253–266.  
570 <https://doi.org/10.1016/j.neuroimage.2017.07.018>
- 571 Tatler, B. W., Wade, N. J., Kwan, H., Findlay, J. M., & Velichkovsky, B. M. (2010). Yarbus,  
572 Eye Movements, and Vision. *I-Perception*, 1(1), 7–27. <https://doi.org/10.1068/i0382>
- 573 Wang, C.-A., Baird, T., Huang, J., Coutinho, J. D., Brien, D. C., & Munoz, D. P. (2018).  
574 Arousal Effects on Pupil Size, Heart Rate, and Skin Conductance in an Emotional  
575 Face Task. *Frontiers in Neurology*, 9, 1029. <https://doi.org/10.3389/fneur.2018.01029>
- 576 Yarbus, A. (1967). *Eye Movements and Vision*. New York, NY: Plenum Press.
- 577 Zhou, B., Bau, D., Oliva, A., & Torralba, A. (2019). Comparing the Interpretability of Deep  
578 Networks via Network Dissection. In W. Samek, G. Montavon, A. Vedaldi, L. K.  
579 Hansen, & K.-R. Müller (Eds.), *Explainable AI: Interpreting, Explaining and*  
580 *Visualizing Deep Learning* (pp. 243–252). Cham: Springer International Publishing.  
581 [https://doi.org/10.1007/978-3-030-28954-6\\_12](https://doi.org/10.1007/978-3-030-28954-6_12)

582

## Appendix

583        Additional analyses were conducted in an attempt to clarify the effect of task on  
 584 classification accuracy. These supplementary analyses were not seen as central to the current  
 585 study, but could prove to be informative to researchers attempting to replicate or extend  
 586 these findings in the future. The results from the primary analysis showed that classification  
 587 accuracies were the lowest for the Memorize condition. To further understand why  
 588 classification accuracy was lower for the Memorize condition than it was for the Search or  
 589 Rate condition, the Exploratory and Confirmatory timeline datasets were systematically  
 590 batched into subsets with the Search (S), Memorize (M), or Rate (R) condition removed (i.e.,  
 591  $\emptyset$ MR, S $\emptyset$ R, SM $\emptyset$ ), and then run through the CNN classifier using the same methods as the  
 592 primary analysis, but with only two classes.

593        All of the data subsets analyzed in this supplementary analysis were decoded with  
 594 better than chance accuracy (see Figure 8a). The same pattern of results was observed in  
 595 both the Exploratory and Confirmatory datasets. When the Memorize condition was  
 596 removed, classification accuracy improved (see Table 4, Figure 8a). When the Rate condition  
 597 was removed, classification was the worst. When the Memorize condition was included (i.e.,  
 598 SM $\emptyset$  and  $\emptyset$ MR), mis-classifications were biased toward Memorize, and the Memorize  
 599 condition was more accurately predicted than the Search and Rate conditions (see Figure 9).

Table 4  
*Supplementary Subset Comparisons*

Comparison	Exploratory		Confirmatory	
	<i>t</i>	<i>p</i>	<i>t</i>	<i>p</i>
$\emptyset$ MR vs. S $\emptyset$ R	3.248	.008	3.094	.012
$\emptyset$ MR vs. SM $\emptyset$	2.875	.021	2.923	.018
S $\emptyset$ R vs. SM $\emptyset$	6.123	< .001	6.017	< .001

600        The accuracies for all of the data subsets observed in the supplementary analysis were  
 601 higher than the accuracies observed in the main analysis. Although there is a clear difference  
 602 in accuracy, the primary analysis was classifying three categories (chance = .33) and the

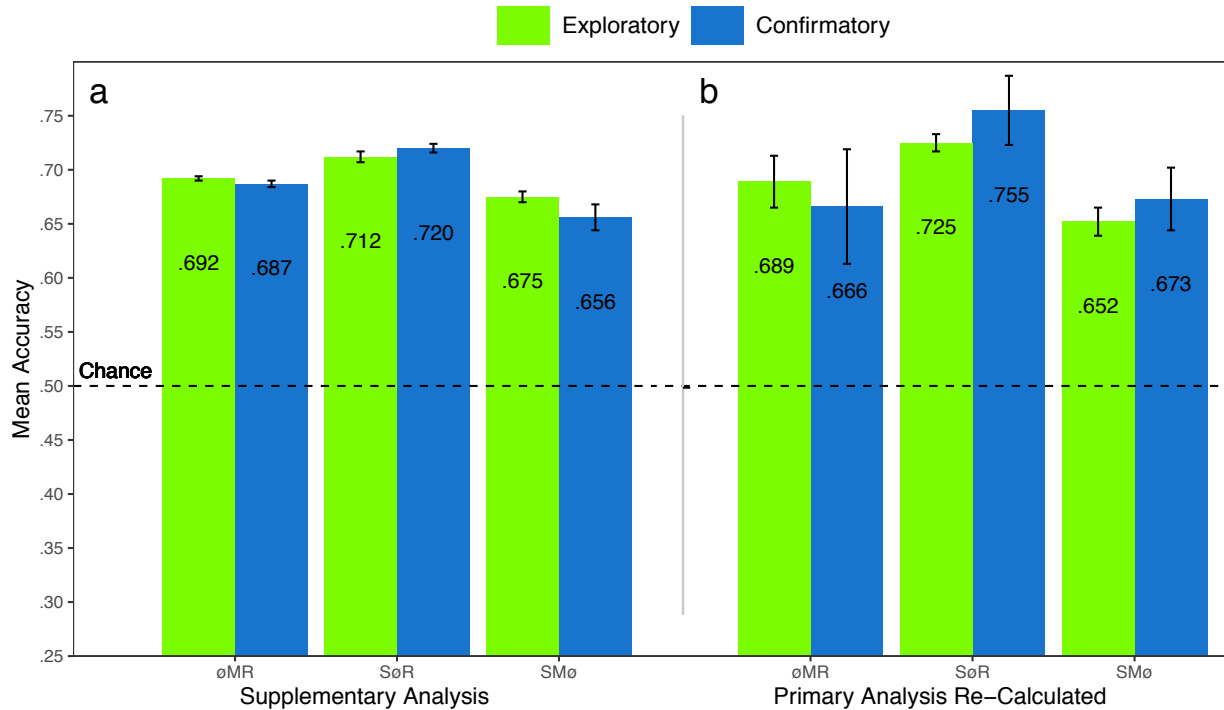


*Figure 8.* The graph represents the average accuracy reported for each subset of the Exploratory and Confirmatory timeline data for (a) the supplementary analysis, and the (b) re-calculated accuracies from the primary analysis. All of the data subsets were decoded at levels better than chance (.50). The error bars represent standard errors.

603 supplementary analysis was classifying two categories (chance = .50). Because the baseline  
 604 chance performance was different for the primary and supplemental analyses, any conclusions  
 605 drawn from a comparison of the results of analyses could be misleading. For this reason, we  
 606 revisited the results from the primary analysis and re-calculated the predictions to be  
 607 equivalent to a 50% chance threshold. Because the cross-validation scheme implemented by  
 608 the DeLINEATE toolbox (<http://delineate.it>; Kuntzelman et al., under review) guaranteed  
 609 an equal number of trials in the test set were assigned to each condition for each dataset, we  
 610 were able to re-calculate 2-category predictions from the 3-category predictions presented in  
 611 the confusion matrices from the primary analysis (see Figure 5). The predictions were  
 612 re-calculated using the following formula:  $\text{Prediction}_{(A,A,A \otimes C)} = \text{Prediction}_{(A,A,ABC)} /$   
 613  $(\text{Prediction}_{(A,A,ABC)} + \text{Prediction}_{(A,C,ABC)})$ . For example, accuracy for the Search  
 614 classification for S $\otimes$ R would be calculated with the following:  $\text{Prediction}_{(S,S,S \otimes R)} =$   
 615  $\text{Prediction}_{(S,S,SMR)} / (\text{Prediction}_{(S,S,SMR)} + \text{Prediction}_{(S,R,SMR)})$ , where  $\text{Prediction}_{(S,R,S \otimes R)}$  is

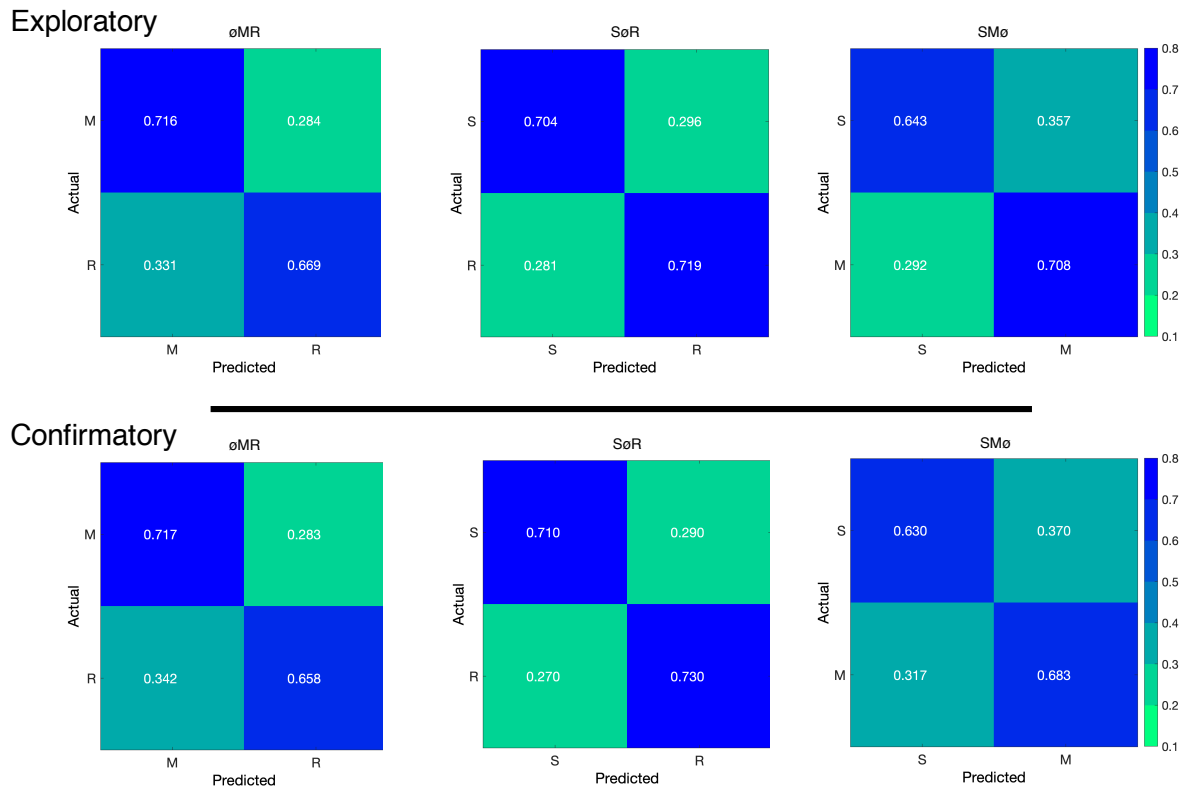


Figure 9. The confusion matrices represent the average classification accuracies for each condition of the timeline data (S = Search, M = Memorize, R = Rate). The vertical axis of the confusion matrices represents the actual condition for the trial. The horizontal axis of the confusion matrices represents the condition that was predicted by the model.

616 the ratio of Search trials that were misclassified as Rate.

617 The results for the re-calculated predictions followed a pattern similar to the main  
 618 supplementary analysis (see Figure 8b). Looking back at the primary analysis, the  
 619 3-category classifications predicted the Memorize conditions with the lowest accuracy (c.f.,  
 620 Search and Rate conditions), and mis-classifications of the Search and Rate conditions were  
 621 most often categorized as Memorize (see Figure 5). Because the Memorize condition was  
 622 mis-classified more often than the other conditions in the primary analysis, the removal of  
 623 the third class in the re-calculated SMø and øMR subsets resulted in a disproportionate  
 624 amount of mis-classified Memorize trials being removed from those data subsets, somewhat  
 625 eliminating the tendency to mis-classify Search and Rate trials as Memorize (see Figure 10).  
 626 Nevertheless, the re-calculated SMø and øMR subsets were classified less accurately than  
 627 SøR, just as in the main supplementary analysis.

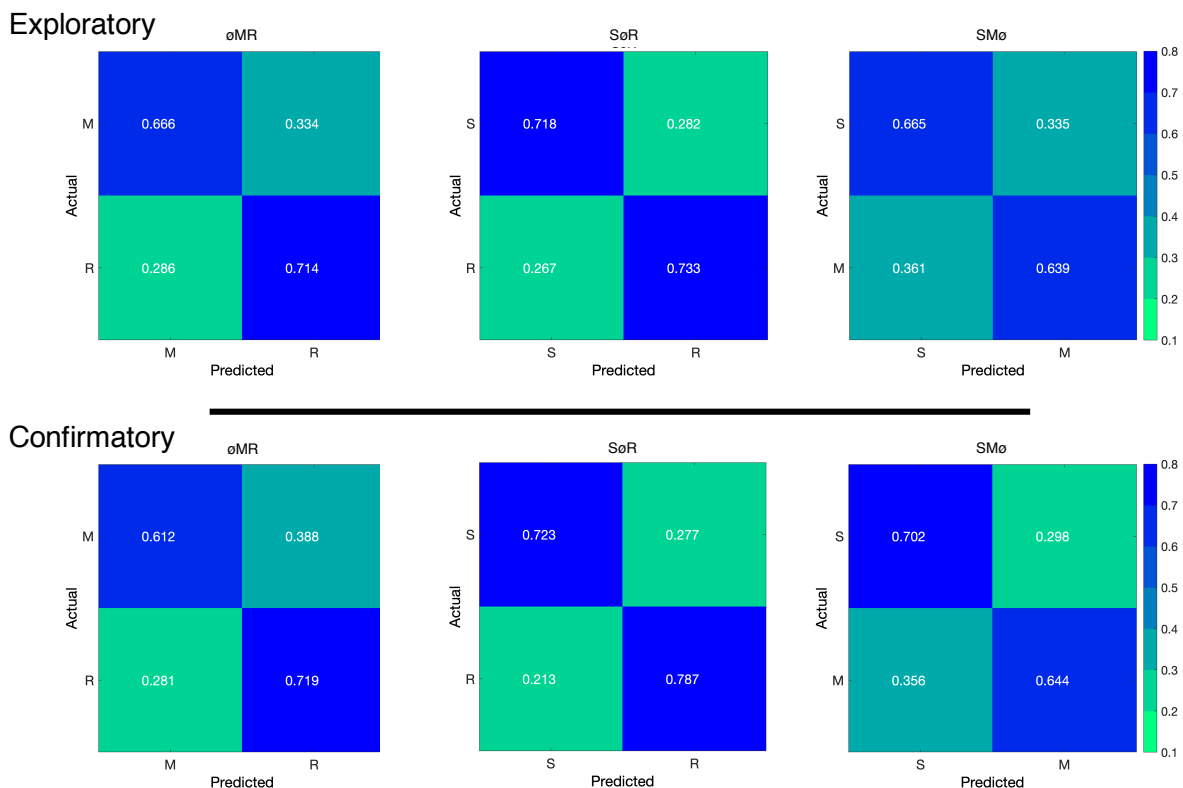


Figure 10. The confusion matrices represent a re-calculation of the classification accuracies for each category from the primary analysis. This re-calculation is meant to make the accuracies presented in the primary analysis (chance = .33) equivalent to the classification accuracies presented in the supplementary analysis (chance = .50).